Journal of Hazardous Materials 169 (2009) 370–375

Contents lists available at ScienceDirect

Journal of Hazardous Materials

journal homepage: www.elsevier.com/locate/jhazmat

Kinetics and oxidative mechanism for H_2O_2-enhanced iron-mediated aeration (IMA) treatment of recalcitrant organic compounds in mature landfill leachate

Yang Deng[a,*], James D. Englehardt[b]

[a] Department of Civil Engineering and Surveying, University of Puerto Rico, PO BOX 9041, Mayaguez, PR 00681, USA
[b] Department of Civil, Architectural and Environmental Engineering, University of Miami, PO BOX 248294, Coral Gables, FL 33124-0630, USA

ARTICLE INFO

Article history:
Received 11 August 2008
Received in revised form 22 March 2009
Accepted 23 March 2009
Available online 31 March 2009

Keywords:
Iron
Hydrogen peroxide
Dissolved oxygen
Recalcitrant organics
Landfill leachate

ABSTRACT

A hydrogen peroxide (H_2O_2)-enhanced iron (Fe^0)-mediated aeration (IMA) process has been recently demonstrated to effectively remove organic wastes from mature landfill leachate. In this paper, the kinetics and oxidative mechanisms of the enhanced IMA treatment were studied. Bench-scale full factorial tests were conducted in an orbital shaker reactor for treatment of a mature leachate with an initial chemical oxygen demand (COD) of 900–1200 mg/L. At the maximum aeration rate (8.3 mL air/min mL sample), process variables significantly influencing the rates of H_2O_2 decay and COD removal were pH (3.0–8.0), initial H_2O_2 doses (0.21–0.84 M), and Fe^0 surface area concentrations (0.06–0.30 m^2/L). Empirical kinetic models were developed and verified for the degradation of H_2O_2 and COD. High DO maintained by a high aeration rate slowed the H_2O_2 self-decomposition, accelerated Fe^0 consumption, and enhanced the COD removal. In hydroxyl radical ($OH^\bullet$) scavenging tests, the rate of removal of glyoxylic acid (target compound) was not inhibited by the addition of para-chlorobenzoic acid ($OH^\bullet$ scavenger) at pH 7.0–7.5, ruling out hydroxyl radical as the principal oxidant in neutral–weakly basic solution. These experimental results show that this enhanced IMA technology is a potential alternative for the treatment of high strength recalcitrant organic wastewaters.

1. Introduction

An iron-mediated aeration (IMA) involving aeration in the presence of micro-scale zero-valent iron process has recently been developed to oxidize EDTA and certain other aqueous organic compounds [1]. In this process, Fe^0 is oxidized by O_2 continuously releasing Fe^{2+}, with simultaneous reduction of some O_2 to H_2O_2. Reactions between Fe^{2+} and H_2O_2 then lead to the production of reactive oxygen species (ROS) responsible for degradation of aqueous organic pollutants. The ROS within the IMA system at acidic condition may be hydroxyl radical ($OH^\bullet$) produced through Fenton chemistry as shown in equation

$$Fe^{2+} + H_2O_2 \rightarrow Fe^{3+} + OH^\bullet + OH^- \quad (1)$$

However, the oxidation at neutral–weakly basic condition is likely associated with the formation of non-hydroxyl radical oxidizing agents, for example, high-valent oxoiron complexes (ferryl) [1–3]. By either postulated pathway, an indispensable step is the Fe^{II}-mediated H_2O_2 formation prior to the production of the ROS. More recently, a H_2O_2-enhanced IMA process has been demonstrated to effectively remove refractory organic wastes in a mature landfill leachate (50% reduction of COD), based on the hypothesis that the direct introduction of H_2O_2 to the IMA process can enhance the oxidation. In addition, 38% of electrical conductivity was reduced due to precipitation, and 83% of ammonia nitrogen was removed by air stripping when the pH was controlled within an appropriate range [4]. In the enhanced IMA process, COD removal efficiency is influenced by iron source, pH, H_2O_2 dose, and aeration rate. The objective of this paper was to investigate the kinetics of H_2O_2 degradation and COD removal, and explore the role of the aeration rate and the oxidative mechanism at neutral–weakly basic pH in the enhanced IMA treatment of a high strength recalcitrant organic wastewater. The effects of pH, H_2O_2 dose, and Fe^0 surface area on the degradation rates of H_2O_2 and COD were assessed through a set of kinetics tests. The role of the aeration rate was revealed through comparison of the rates of H_2O_2 decay, iron corrosion, and COD removal at various aeration rates. Finally, hydroxyl radical scavenging tests were conducted to identify the ROS under neutral–weakly basic conditions.

2. Experimental

2.1. Mature landfill leachate and reagents

All chemicals were at least analytical grade except as noted, and were used as received. A landfill leachate was collected from North

* Corresponding author. Tel.: +1 787 832 4040x2131; fax: +1 787 833 8260.
E-mail addresses: yang.deng@upr.edu, dengyang7@yahoo.com (Y. Deng).

0304-3894/$ – see front matter © 2009 Elsevier B.V. All rights reserved.
doi:10.1016/j.jhazmat.2009.03.106

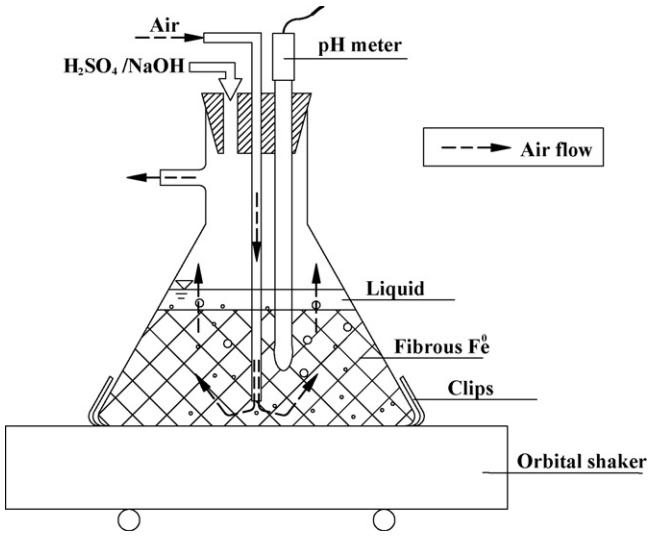

Fig. 1. IMA orbital shaker reactor.

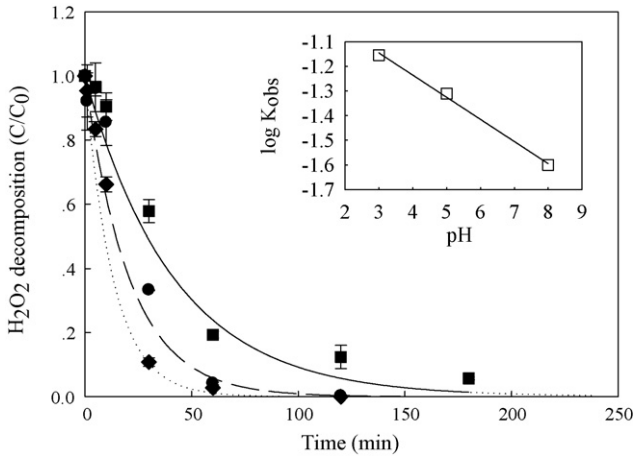

Fig. 2. H_2O_2 decomposition versus time at pH 3 (♦ ...), 5 (● --), and 8 (■– –). (Conditions: $[H_2O_2]_0 = 0.63$ M; aeration rate = 8.3 mL air/min mL sample; $[Fe^0_{surf}] = 0.15\ m^2/L$; $COD_0 = 1119$ mg/L.) Symbols and lines represent the measured data and the fit of the hypothetical reaction model, respectively.

Central Landfill in Polk County (Winter Haven, FL). The average composition of the tested landfill leachate COD were as follows: COD, 900–1200 mg/L; electrical conductivity, 8.30 ms/cm; pH, 8.2; and the mean BOD_5/COD, 0.02. The leachate was collected in a zero headspace plastic bottle and refrigerated at 4 °C until use. Brillo® fibrous iron (Fe^0) (Church & Dwight Co., Princeton, NJ) was used as reactive iron media (11.70 m^2/kg nominal specific surface area based on fiber diameter measurement). Hydrogen peroxide (H_2O_2, VWR, West Chester, PA) was purchased and used as a 30% (w/w) solution. Glyoxylic acid (glyoxylic acid monohydrate, 97%, Alfa Aesar) and para-chlorobenzoic acid (pCBA) (98%, Alfa Aesar) were purchased from VWR.

2.2. Experimental setup

The IMA orbital shaker reactor using fibrous media is shown in Fig. 1. A designated amount of fibrous iron was prepared by hexane rinse, complete drying, 0.1 N HCl rinse, and final drying, and then formed to a relatively uniform fiber density in the flask. Forty milliliters of the sample mixed with a known amount of H_2O_2 (30%, w/w) was dispensed into a 50 mL glass side arm flask installed in an orbital shaker (G24 environmental incubator shaker, New Brunswick Scientific Co., Inc., Edison, NJ, USA) at 200 rpm. Aeration was continuously provided through a glass tube by an air pump (AP200, Tetratec, China). Rapid shaking and continuous aeration ensured complete mixing conditions. In the leachate treatment tests, a pH meter probe (model 370, ORIN) was inserted into the solution to monitor sample pH. Concentrated sulfuric acid and 10 M NaOH were used to adjust the initial pH of the leachate sample, and to maintain the desired pH during the experiment if necessary. In the hydroxyl radical scavenging tests, pH was not controlled.

2.3. Experimental procedure and sample preparation

In the leachate treatment tests, 2 mL of homogenized solution was taken from the fibrous iron orbital shaker reactors at the designated reaction time. Five hundred microliter of the sample was used to test residual H_2O_2, and 30 μl was prepared for total iron analysis. The remaining sample was heated in a 50 °C water bath for 30 min to remove residual H_2O_2, and vacuum filtered through a 0.45 μm Millipore filter membrane. A set of comparative tests validated that the measured COD was not lowered by use of the membrane filtration. Finally, the filtrate was prepared for COD testing to determine the total COD removal efficiency. In hydroxyl radical scavenging tests, the experimental setup was the same as in the leachate treatment tests. Glyoxylic acid (GA) and p-chlorobenzoic acid (pCBA) were the target compound and the OH• scavenger, respectively. Four groups of tests with an initial GA concentration of 0.20 mM were conducted to compare the degradation rates of GA: IMA alone (no H_2O_2), H_2O_2 alone (no Fe^0), H_2O_2-enhanced IMA, and H_2O_2-enhanced IMA + 0.26 mM pCBA.

2.4. Analytical methods

BOD_5 was measured according to standard method 5210 B [5]. COD was measured colorimetrically using COD digestion vials (high range, 20–1500 mg/L, HACH, Loveland, CO). H_2O_2 was measured by the titrimetric method [6]. The homogenized sample of 0.03 mL for total iron analysis was digested and diluted as described previously [4]. Total iron was measured by flame atomic absorption spectrometry (Analyst 800, PerkinElmer). Glyoxylic acid was determined by UV–vis spectrophotometry by the method of Caprio and Insola [7]. Error bars shown in all the figures represent one standard deviation ($n \geq 2$).

3. Results and discussion

3.1. H_2O_2 decomposition

H_2O_2 decomposition as a function of time at various pH values is shown in Fig. 2. At pH 3, 5, and 8, H_2O_2 exhibited a pseudo-first-order decay with observed rate constants (k_{obs1}) of 0.070, 0.049, and 0.025 min^{-1}, respectively. The rate of H_2O_2 decomposition increased with the decreasing pH. Generally speaking, H_2O_2 is more stable in the absence of Fe^0 under acidic condition than at neutral or alkaline condition [8]. However, in the test using Fe^0, elemental iron could react with H^+ under acidic condition to produce Fe^{2+} and release H_2 gas (Eq. (2)).

$$Fe^0 + 2H^+ \rightarrow Fe^{2+} + H_2 \quad (2)$$

Apparently, low pH produced more Fe^{2+}, catalyzing H_2O_2 decomposition via Eq. (1). Thus, a higher H_2O_2 decomposition rate was achieved at pH 3 than at pH 8.

H_2O_2 decomposition as a function of time at various $[H_2O_2]_0$ and $[Fe^0_{surf}]$ are shown in Figs. 3 and 4, respectively. At any particular $[H_2O_2]_0$ or $[Fe^0_{surf}]$, a pseudo-first-order of H_2O_2 decomposition was observed. Lower $[H_2O_2]_0$ and higher $[Fe^0_{surf}]$ led to a faster H_2O_2 decay. The H_2O_2 decay in the H_2O_2-enhanced IMA treatment of

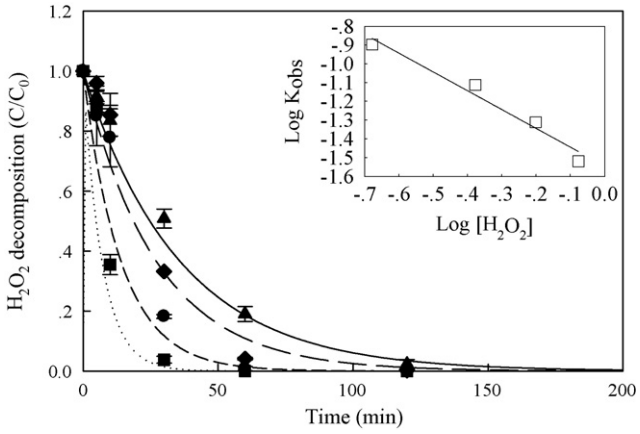

Fig. 3. H_2O_2 decomposition versus time at $[H_2O_2]_0$ of 0.21 (■ . . .), 0.42 (● - -), 0.63 (♦ – – –), and 0.84 M (▲—). (Conditions: pH 5; aeration rate = 8.3 mL air/min mL sample; $[Fe^0_{surf}] = 0.15\ m^2/L$; $COD_0 = 1119$ mg/L). Symbols and lines represent the measured data and the fit of the hypothetical reaction model, respectively.

the leachate was modeled, assumed as a function of hydrogen ion ($[H^+]$), initial H_2O_2 dose ($[H_2O_2]_0$), and nominal Fe^0 surface area concentration ($[Fe^0_{surf}]$), as shown:

$$\frac{d[H_2O_2]}{dt} = -k_{H_2O_2}[H^+]^a[H_2O_2]_0^b[Fe^0_{surf}]^c[H_2O_2] \quad (3)$$

In the initial reaction phases at different pH (Fig. 2), $[Fe^0_{surf}]$ and $[H_2O_2]$ were not greatly changed, and the Eq. (3) could be approximately expressed as $d(dt/[H_2O_2]) = -k_{obs}[H^+]^a$. A log–log linear

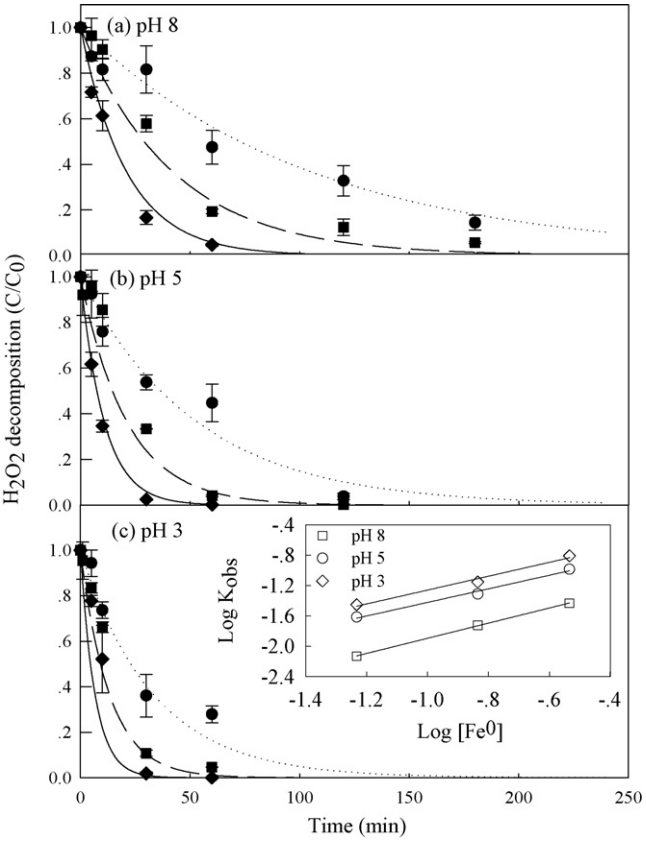

Fig. 4. H_2O_2 decomposition versus time at $[Fe^0_{surf}]$ of 0.6 (■ . . .), 0.15 (● - -), and 0.30 (♦ – – –) m^2/L (Conditions: $[H_2O_2]_0 = 0.63$ M; aeration rate = 8.3 mL air/min mL sample; $COD_0 = 1119$ mg/L): (a) pH 8; (b) pH 5; and (c) pH 3. Symbols and lines represent the measured data and the fit of the hypothetical reaction model, respectively.

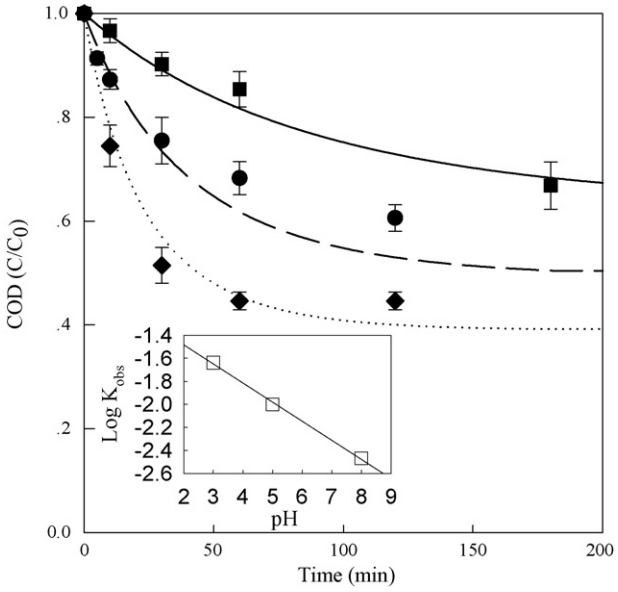

Fig. 5. COD versus time at pH 3 (♦ . . .), 5 (● - -), and 8 (■–). (Conditions: $[H_2O_2]_0 = 0.63$ M; aeration rate = 8.3 mL air/min mL sample; $[Fe^0_{surf}] = 0.15\ m^2/L$; $COD_0 = 1119$ mg/L). Symbols and lines represent the measured data and the fit of the hypothetical reaction model, respectively.

dependence of rate of k_{obs} on pH was observed in the insert of Fig. 2. Therefore, $a = 0.1$, the slope of the straight line in the insert of Fig. 2). In a similar way, we determined $b = -1$, and $c = 1$. Finally, $k_{H_2O_2} = 0.62$.

Since the reactor was operated in a batch mode, $[H_2O_2]$ at any time t could be expressed as Eq. (4) for constant pH and $[Fe^0_{surf}]$ after integration.

$$[H_2O_2] = [H_2O_2]_0 e^{-0.62[Fe^0_{surf}][H^+]^{0.1}/[H_2O_2]_0 t} \quad (4)$$

Chi-square tests were used to evaluate the fit of the model. The chi-square goodness of fit test was computed as

$$\chi^2 = \sum_{i=1}^{n} \frac{(\text{observed value}_i - \text{expected value}_i)^2}{\text{expected value}_i} \quad (5)$$

in which the observed values were the measured $[H_2O_2]$, and the expected values were the modeled $[H_2O_2]$. The criterion for acceptable fit was:

$$P(\chi^2 \le \chi_0^2) = 1 - \alpha \quad (6)$$

in which α is the confidence level and χ_0^2 is the chi-square cumulative distribution value for $n-1$ degree of freedom. At a 95% confidence level, all models satisfied $\chi^2 \le \chi_0^2$, indicating fit test at a 0.05 significance level, as also shown in Figs. 2–4.

3.1.1. COD removal

Overall COD removal as a function of time at various pH values is shown in Fig. 5. At any particular pH tested, COD removal exhibited a pseudo-first-order degradation. A higher rate of COD removal was achieved at low pH, implying that high $[H^+]$ favored the generation of the ROS. This observation may be explained in terms of three factors. First, more Fe^{2+} was produced at a low pH via Eq. (2). Second, Fe^{2+} was more soluble at a low pH (particularly < 4.0) [9]. Third, less iron sludge was precipitated on the Fe^0 surface to inhibit the IMA process at a low pH. COD removal rates versus time at various $[H_2O_2]$ and $[Fe^0_{surf}]$ are shown in Figs. 6 and 7, respectively. COD removal was observed to be a pseudo-first-order reaction with respect to $[H_2O_2]$ and $[Fe^0_{surf}]$. H_2O_2 was apparently the key reactant

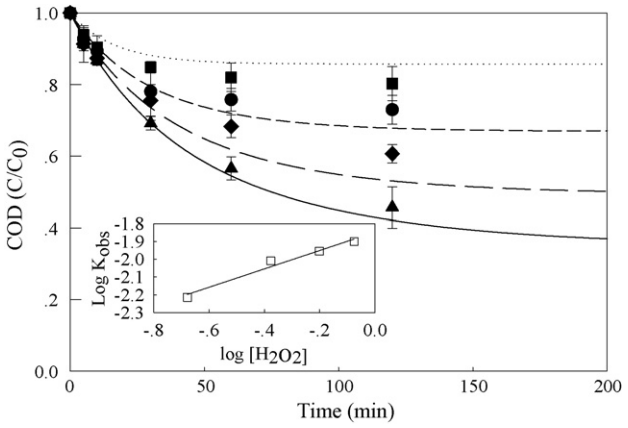

Fig. 6. COD versus time at $[H_2O_2]_0$ of 0.21 (■ ...), 0.42 (● --), 0.63 (♦ – – –), and 0.84 (▲—) M. (Conditions: pH 5; aeration rate = 8.3 mL air/min mL sample; $[Fe^0_{surf}]$ = 0.15 m^2/L; COD_0 = 1119 mg/L): (a) overall; (b) oxidation. Symbols and lines represent the measured data and the fit of the hypothetical reaction model, respectively.

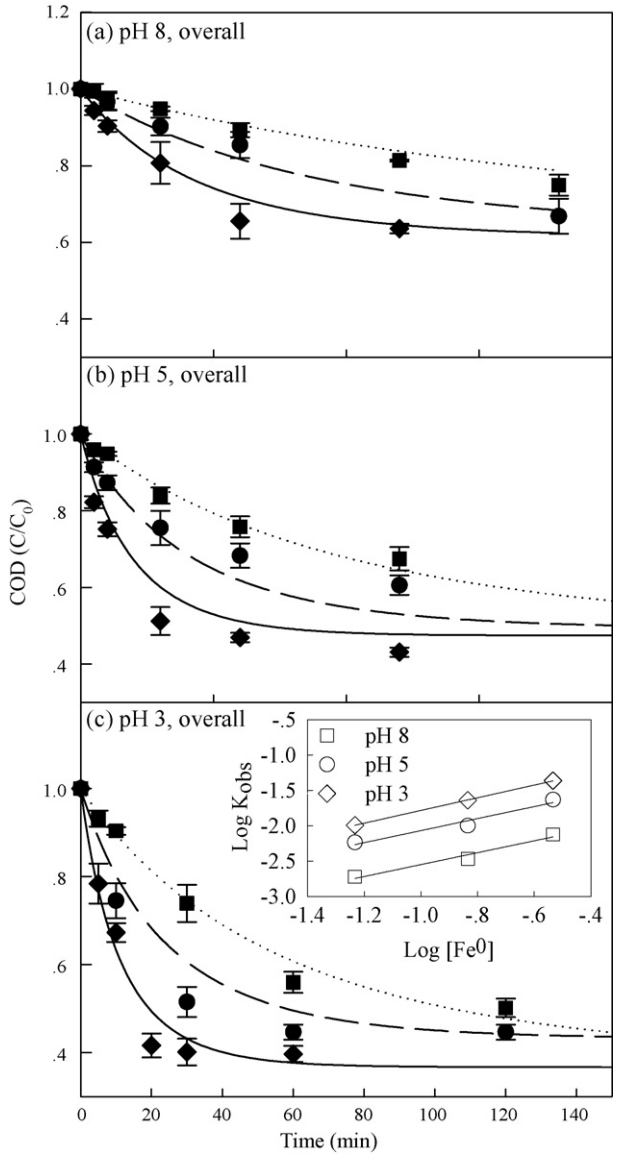

Fig. 7. COD removal versus time at $[Fe^0_{surf}]$ of 0.06(■ ...), 0.15 (● --), and 0.30 (♦ – – –) m^2/L and various pH. (Conditions: $[H_2O_2]_0$ = 0.63 M; aeration rate = 8.3 mL air/min mL sample; COD_0 = 1119 mg/L). Symbols and lines represent the measured data and the fit of the hypothetical reaction model, respectively.

to produce the ROS in the presence of iron ions, and a high H_2O_2 concentration also could enhance the formation of Fe^{2+} via Eq. (7).

$$Fe^0 + H_2O_2 \rightarrow Fe^{2+} + 2OH^- \quad (7)$$

In addition, high $[Fe^0_{surf}]$ corresponds to a larger Fe^0 surface and more active sites on which the Fe^{2+} and ROS are produced.

COD removal, assumed as a function of $[H^+]$, H_2O_2 concentration ($[H_2O_2]$), and $[Fe^0_{surf}]$, was modeled as follows:

$$\frac{dCOD}{dt} = -k_{COD}[H^+]^d[H_2O_2]^e[Fe^0_{surf}]^f COD \quad (8)$$

where $d = 0.16$, $e = 0.40$, $f = 1.0$, and $k_{COD} = 0.70$ using the similar methods used to determine the reaction orders in the H_2O_2 decomposition kinetic model. Considering the reactor was operated in batch mode, residual COD after integration could be expressed as

$$COD = COD_0 e^{2.82[H^+]^{0.06}[H_2O_2]_0^{1.4}(e^{-0.248(Fe^0[H^+]^{0.1}/[H_2O_2]_0)t}-1)} \quad (9)$$

At a 95% confidence level, all models satisfied $\chi^2 \leq \chi^2_0$, indicating fit at a 0.05 significance level. These fits are also shown in Figs. 5–7.

3.1.2. Role of aeration

Aeration rates in the range of 0–8.3 mL air/min mL sample were tested in the H_2O_2-enhanced IMA treatment of leachate (Fig. 8a–c). As seen in Fig. 8a, H_2O_2 decay was independent of the aeration rate within the first 30 min, but thereafter a higher aeration rate slowed the H_2O_2 decay. This inhibiting effect was likely attributable to two factors. First, the H_2O_2 was decomposed through at least two pathways: through production of the ROS, and through H_2O_2 self-decomposition (constituting a waste of bulk oxidant) as in Eq. (10).

$$2H_2O_2 \leftrightarrow 2H_2O + O_2 \quad (10)$$

Apparently, a high DO level maintained by a high aeration rate favored a shift of reaction (10) toward the left side to slow the H_2O_2 self-decomposition. Second, high aeration rate caused more rapid Fe^0 corrosion as shown in Fig. 8b. Thus, larger amounts of iron sludge accumulated on the Fe^0 surface, preventing H_2O_2 access to Fe^0 and decreasing H_2O_2 decomposition.

Fe^0 consumption at various aeration rates is shown in Fig. 8b. Although a high aeration rate led to a lower H_2O_2 decomposition rate, the amount of consumed Fe^0 increased with increasing aeration rate (Fig. 8b), implying that a fraction of the consumed Fe^0 was due to oxidation by another oxidant, molecular oxygen. Of note, a similar trend in the Fe^0 consumption rate was observed for all the aeration rates: Fe^0 consumption increased rapidly within the first 30 min, then more slowly until 120 min, and again dramatically thereafter. Such variation in Fe^0 consumption seemed to be related to the buildup and destruction of an iron sludge layer on the Fe^0 surface. Initially, Fe^0 was rapidly oxidized by H_2O_2 and O_2, causing a sharp increase in Fe^0 consumption within the first 30 min. As the Fe^0 surface was progressively covered by the iron sludge layer, Fe^0 oxidation was gradually inhibited. Such inhibition might be particularly serious in the presence of H_2O_2 at weakly basic pH. However, the sludge layer might be destroyed by some species present in leachate to again promote the Fe^0 corrosion. For example, Cl^- has a well-known depassivation effect [10].

COD removal at different aeration rates is shown in Fig. 8c. Within the first 30 min, no significant difference in COD removal was observed for the tested groups. However, COD removal became slower at lower aeration rate thereafter, suggesting the involvement of H_2O_2 in ROS formation.

Aeration played an important role in treatment, differentiating the H_2O_2-enhanced IMA process from traditional Fenton treatment using Fe^0. Based on these results, high aeration rates eventually led

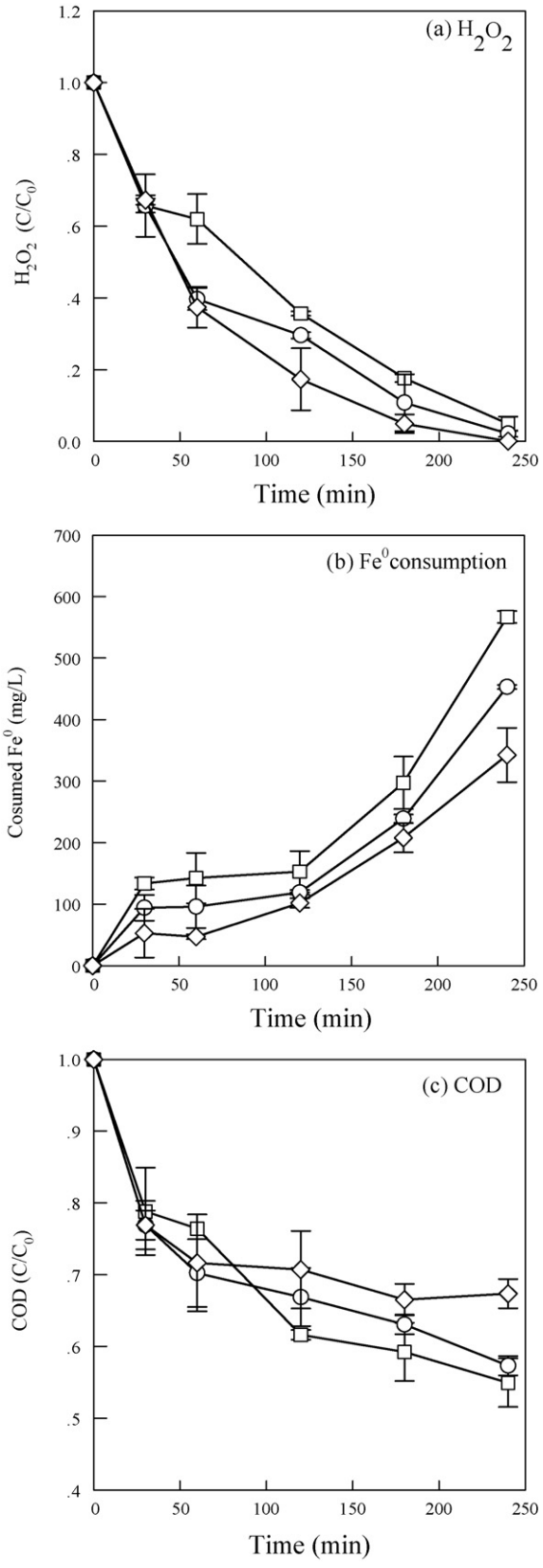

Fig. 8. H_2O_2-enhanced IMA treatment of leachate at various aeration rates of 0 mL air/min mL sample (◊), 4.17 mL air/min mL sample (○), and 8.3 mL air/min mL sample (□): (a) H_2O_2 decomposition; (b) Fe^0 consumption; (c) COD. (Conditions: $[H_2O_2]_0$ = 0.84 M; $[Fe^0_{surf}] = 0.17\ m^2/L$; COD_0 = 935 mg/L.)

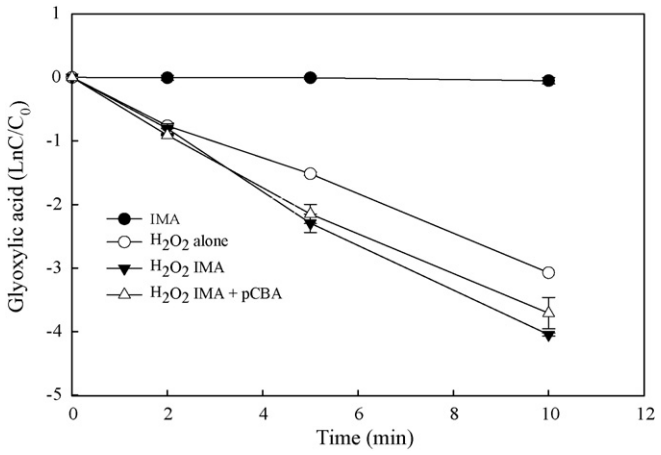

Fig. 9. Glyoxylic acid removal versus time in enhanced-IMA at various conditions: IMA, H_2O_2 treatment alone, H_2O_2-enahnced IMA, and H_2O_2-enahnced IMA + 0.26 mM pCBA. (Conditions: pH 7.0–7.5; $[Fe^0_{surf}] = 0.09\ m^2/L$; aeration rate = 4.17 mL air/min mL sample; initial glyoxylic acid concentration = 0.20 mM.)

to high COD removal rates, for two possible reasons. First, as mentioned above, a high DO maintained by a high aeration rate inhibited the H_2O_2 self-decomposition, perhaps enhancing production of the principal ROS. Second, DO might participate in the oxidation of Fe^0 to Fe^{2+}, perhaps contributing to enhanced ROS yield.

3.1.3. *Oxidative mechanism at neutral–weakly acidic pH*

In our previous studies [1] to detect OH• at pH 7.5 during IMA treatment, the degradation of GA (the target compound) was not slowed when pCBA (the OH• scavenger) was present, effectively ruling out OH• as an oxidant. However, the species of ROS active in H_2O_2-enhanced IMA have not been investigated at neutral pH. In this study, a set of OH• scavenger tests for the H_2O_2-enhanced IMA process was conducted at pH 7.0–7.5 (Fig. 9). The rate constants for the reactions of GA and pCBA with OH• are 3.6×10^8 and $5.0 \times 10^9\ M^{-1}\ s^{-1}$, respectively. If hydroxyl radicals were the principal oxidant, the decomposition rate of 0.26 mM GA without pCBA would be 18 times higher than that with 0.20 mM pCBA. As shown in Fig. 9, although simple H_2O_2 treatment could decompose GA, higher decomposition efficiencies were shown for the H_2O_2-enhanced IMA groups with and without pCBA, implying that additional oxidants were generated. Furthermore, no significant difference in the additional GA decomposition rates was observed in the presence and absence of pCBA, particularly in the initial reaction stage (within the first 5 min), suggesting that OH• was not the principal oxidant in the H_2O_2-enhanced IMA process at neutral–weak basic pH.

4. Conclusion

Based on these laboratory tests, the H_2O_2-enhanced IMA process can remove COD impurities in landfill leachate. The rates of H_2O_2 decomposition and COD removal depended primarily on pH, initial H_2O_2 dose, and Fe^0 surface area concentration. Since aeration rate controlled the DO level, it was an essential factor for the enhanced treatment, in agreement with our previous finding [4]. High aeration rate apparently inhibited the H_2O_2 self-decomposition, perhaps partially replaced H_2O_2 to promote yield of the principal ROS, and accelerated the oxidation of organic compounds. Scavenging tests indicated non-hydroxyl radical oxidizing species under neutral–weakly basic conditions, consistent with observations of the IMA system [1].

These results augment knowledge of the kinetics and oxidative mechanisms of the H_2O_2-enahnced IMA process, further demon-

strating that the technology may result attractive for the treatment of landfill leachate, provided that it is further tested and optimized.

Acknowledgments

This work was funded in part by Hinkley Center for Solid and Hazardous Waste Management, and in part by the University of Miami. Jose Polar and Samer Abdul Aziz are kindly appreciated for their unselfish help with the laboratory tests.

References

[1] J. Englehardt, D. Meeroff, L. Echegoyen, Y. Deng, F. Raymo, T. Shibata, Oxidation of aqueous EDTA and associated organics and coprecipitation of inorganics by ambient iron-mediated aeration, Environ. Sci. Technol. 41 (1) (2007) 270–276.
[2] S.J. Hug, O. Leupin, Iron-catalyzed oxidation of arsenic(III) by oxygen and by hydrogen peroxide: pH-dependent formation of oxidants in the Fenton reaction, Environ. Sci. Technol. 37 (2003) 2734–2742.
[3] C. Keneen, D. Sedlak, Factors affecting the yield of oxidants from the reaction of nanoparticulate zero-valent iron and oxygen, Environ. Sci. Technol. 42 (2008) 1262–1267.
[4] Y. Deng, J. Englehardt, Hydrogen peroxide-enhanced iron-mediated aeration for the treatment of mature landfill leachate, J. Hazard. Mater. 153 (2008) 293–299.
[5] APHA, AWWA, WEF, Standard Methods for the Examination of Water and Wastewater, 19th ed., APHA, 1995.
[6] I.M. Kolthoff, E.B. Sandell, Textbook of Quantitative Inorganic Analysis, third ed., The Macmillan Company, New York, NY, 1952.
[7] V. Caprio, A. Insola, A revised method for the spectrophotometric determination of glyoxylic-acid, Anal. Chim. Acta. 189 (1986) 379–382.
[8] R.E. Meeker, Stabilization of hydrogen peroxide, US Patent 3,208,606 (1965).
[9] J. Pignatello, E. Oliveros, A. MacKay, Advanced oxidation processes for organic contaminant destruction based on the Fenton reaction and related chemistry, Crit. Rev. Environ. Sci. Technol. 36 (1) (2006) 1–84.
[10] S. Ahn, H. Kwon, D.D. Macdonald, Role of chloride ion in passivity breakdown on iron and nickel, J. Electrochem. Soc. 152 (11) (2005) B482–B490.